PCCP

RSC Publishing

PAPER

Improving the antifouling property of polysulfone ultrafiltration membrane by incorporation of isocyanate-treated graphene oxide

Cite this: *Phys. Chem. Chem. Phys.*, 2013, **15**, 9084

Haiyang Zhao,[a] Liguang Wu,[b] Zhijun Zhou,[a] Lin Zhang*[a] and Huanlin Chen[a]

Received 4th March 2013,
Accepted 5th April 2013

DOI: 10.1039/c3cp50955a

www.rsc.org/pccp

In this paper, isocyanate-treated graphene oxide (iGO), which can be well dispersed in organic solvent, was prepared in a simple manner and showed excellent compatibility with polysulfone (PSF). iGO–PSF ultrafiltration membranes were prepared by the classical phase inversion method. The separation performance and the antifouling property of the prepared membranes were investigated in detail. The antifouling property of the prepared membranes was found to be greatly enhanced by the addition of iGO, and we attributed the enhanced antifouling property to the improved hydrophilicity, the more negative zeta potential and the improved smoothness of the membrane surface.

Introduction

The achievement of mechanical exfoliation of single-layer graphene in 2004,[1] as a one-atom-thick sheet of sp^2-bonded hexagonal carbon atom lattice,[2,3] initiated a rush on the exploitation of this fascinating nanomaterial with exceptional chemical,[4–7] electrical,[8,9] thermal[10] and mechanical[11] properties.

Although pristine graphene has been endowed with unparalleled properties, it is also reported that original graphene is chemically inert and slightly dissolves in typical organic solvents.[12] Therefore appropriate chemical modification is necessary in order to use pristine graphene in practical applications.[12,13] Fortunately, the normal route to preparing graphene is the chemical exfoliation of graphite (*i.e.* Hummers method),[14,15] which grants graphene abundant amounts of hydroxyl, epoxy and carboxylic groups.[7,13] The graphene prepared by this method is highly oxidized and has numerous defects, generally called graphene oxides (GO).[7] The obtained GO can be reduced to graphene by hydrazine vapor,[12] or further modified by covalent modification by the amidation of carboxylic or epoxy groups,[16,17] non-covalent functionalization of graphene,[18] *etc*. Stankovich *et al.*[19,20] reported on the modification of GO using organic isocyanate, and found that the surface modification reduced the hydrophilic character of GO sheets by forming amide and carbamate ester bonds with the carboxyl and hydroxyl groups, respectively.

Several special properties of modified graphene have also been investigated, including the optical properties mediated by pH,[21] the biocompatible property for adhesion and proliferation of L-929 cells,[22] the transport property as an effective nanocargo to deliver water-insoluble drugs into cells, and the unquestionable antibacterial properties.[23–27]

Despite the attention graphene has caused, the application of graphene to separation membrane materials has been barely examined. Recently, Geim and his group[28] fabricated a GO-based membrane with the competence of unimpeded permeation of water vapor but almost total retention of other gas species. Cohen-Tanugi and Grossman simulated the capability of etched graphene to remove salt as a reverse osmosis membrane, and their work was highlighted by Wang and Karnik.[29] Therefore, it is believed that graphene could improve separation membranes of elaborate design. But it is quite difficult to put this idea into effect as carbon nanotubes (CNTs)[30,31] because no natural water tunnel exists in GO. However, GO may also have some other effects on the practical performance of a GO/polymer hybrid membrane, such as on the surface charge, antifouling and mechanical properties.

In this paper, for the sake of incorporating graphene into membranes to improve their performance, we focused on the modification of GO by isocyanate treatment. Isocyanate-treated GO (iGO) displayed good dispersant ability in organic solution and excellent compatibility with polymeric components. Subsequently, membranes of polysulfone (PSF) loaded with iGO were prepared by a classical phase-inversion method. The properties of the

[a] *Key Laboratory of Biomass Chemical Engineering of Ministry of Education, Department of Chemical and Biological Engineering, Zhejiang University, Hangzhou, 310027, P. R. China. E-mail: linzhang@zju.edu.cn; Fax: +86 571 8795 3802; Tel: +86 571 8795 3802*

[b] *College of Environmental Science & Engineering, Zhejiang Gongshang University, Hangzhou, 310035, P. R. China*

membrane were observed by a scanning electron microscope (SEM) and atomic force microscopy (AFM). The separation performance and antifouling property of the prepared membrane were investigated in detail.

Experimental

Materials and reagents

Graphene oxide (GO), with diameters between 1 and 5 μm and 99% purity, was manufactured by XFNANO Material Tech Co., Ltd., China. The classical Hammers Method was utilized in the oxidization process of GO.[14,15] Analytical grade dimethylformamide (DMF), polyvinyl pyrrolidone (PVP), Bull Serum Albumin (BSA), and ovalbumin, were purchased from Shanghai Reagent Company, China. Polysulfone (PSF) was purchased from BASF. Analytical grade 4-acetylphenyl isocyanate was bought form Sigma-Aldrich. The microfiltration membrane, with a pore diameter of 0.45 μm, was purchased from Whatman.

Preparation of isocyanate-treated GO

As referred to in Stankovich's procedure,[19] GO (150) mg was loaded into a round bottom flask (25 mL) equipped with a magnetic stir bar, and then the 4-acetylphenyl isocyanate (6 mmol) was added. Anhydrous DMF (15 mL) then followed under nitrogen to create an inhomogeneous suspension, and the mixture was allowed to stir under the protection of nitrogen for 24 h at ambient temperature. After the slurry reaction, the mixture was poured into methylene chloride (150 mL) in order to coagulate. Then the product was filtered with a 0.45 μm filter membrane, rinsed with additional methylene chloride (150 mL), and dried in a vacuum.

Preparation of iGO-doped membrane

Asymmetric iGO–PSF ultrafiltration membranes were prepared by the phase-inversion method. This involved preparing a casting solution composed of PSF (18 wt%), and PVP (1 wt%) in DMAC as solvent. Precise amounts of iGO (0.025, 0.05, 0.10 and 0.15 wt%) were dispersed into corresponding amounts of DMAC to prepare iGO solutions, and sonicated for 1 h for adequate dispersion. Note that membranes marked as 0.15% refer to membranes prepared in a casting solution in which the content of the iGO with respect to PSF + PVP + DMAC was 0.15%. After the dispersion of iGO in DMAC, PSF and PVP were dissolved in the dope solution by continuous stirring for 24 h. The resultant homogeneous polymeric solution was cast on a clear glass plate, and subsequently immersed into a coagulation bath (deionized water, at 25 °C). After a few minutes, a thin membrane separated from the glass. The membranes obtained were soaked in deionized water for at least 24 h at room temperature to guarantee complete phase separation.

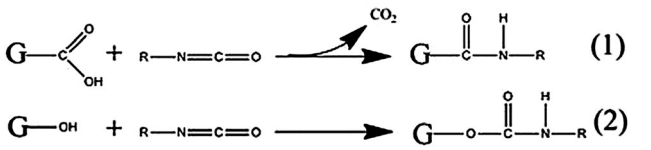

Fig. 1 Possible reactions during the isocyanate treatment of GO, where organic isocyanate reacted with the hydroxyl and carboxyl groups.

Characterization of modified iGO and iGO-doped membrane

The functional groups and structure differences of GO and iGO were characterized by FTIR (Tense 27, Bruker, France) and Raman spectroscopy (DXR532, Thermo Fisher, US). FTIR spectra were also recorded to characterize the presence of iGO in the iGO–PSF membrane. To investigate the surface chemistry, X-ray photoelectron spectra (XPS, Kratos Axis Ultra DLD, Japan) were recorded using a Kratos Axis Ultra DLD spectrometer employing a monochromated Al Kα X-ray source ($h\nu$ = 1486.6 eV), hybrid (magnetic/electrostatic) optics, and a multichannel plate and delay line detector (DLD). All X-ray photoelectron spectra were recorded using an aperture slot of 300 × 700 μm^2, survey spectra were recorded with pass energy of 160 eV, and high-resolution spectra were recorded with pass energy of 40 eV. The electron emission gives a sampling depth of 10 nm.

A scanning electron microscope (SEM, Utral 55, CorlzeisD, Germany) directly provided the visual information of the surface and cross-sectional morphology of the membrane. The membranes were cut into small pieces, and then the sample pieces were immersed into liquid nitrogen for 60 s and broken by a pair of tweezers. Then the samples were kept in air for drying. The dried samples were glued to the stages with conductive tape and sputtering with gold to produce the conductivity.

Membrane hydrophobicity was measured by the contact angle that was formed between the membrane and water with the assistance of a contact angle meter (Digidrop, GBX, France) equipped with video capture at room temperature. Before measurement, the membranes were kept in vacuum at 40 °C for 12 h to obtain dry samples of a constant weight. A total of 1 μL of deionized water was dropped onto a dry membrane surface with a microsyringe. At least 10 contact angles were averaged to obtain a reliable value.

The equilibrium water content of the membranes was also tested. Pre-weighed membranes, kept in desiccators to desorb any moisture from the air, were immersed in deionized water in a closed system at 25 °C for 24 h. Then the membranes were taken out and carefully wiped to remove any solution on the surface and weighed. The equilibrium water content (EWC, %) was calculated by:

$$\mathrm{EWC}(\%) = \frac{W_{\mathrm{wet}} - W_{\mathrm{dry}}}{W_{\mathrm{dry}}} \times 100 \qquad (1)$$

where W_{wet} and W_{dry} are the weights of the swollen and dry membranes, respectively.

The electrical property of the membrane surface is an important characterization to interpret and predict the filtration process, especially with regard to fouling.[32–34] One common way to evaluate the electrical property of the membrane surface and the solute–membrane interaction is by the zeta potential.[35–42] In this paper, the zeta potential of the prepared membranes was measured with a SurPASS instrument (Anton Paar GmbH, Austria). The wet membrane samples were cut into rectangular

profiles according to the template module and soaked in pure water before measurement. Thus, before each measurement two pieces of composite membranes were mounted and soaked for at least 30 min in the electrolyte solution (solution of KCl, 1 mM, pH = 7). This solution was prepared using ultra-purity water (milli-Q, Millipore, US). Another rinse and flow check was needed before the measurement of the zeta potential.

Characterization of membrane separation performance

The separation performance of prepared ultrafiltration membranes was characterized by measuring the pure water flux, BSA (molecular weight: 6700) and ovalbumin (molecular weight: 4500) rejection in a cross flow test system under 25 °C and 100 kPa. Each membrane was supported in the cell on a porous stainless steel disk where the effective area of the membrane was 22.1 cm^2. Pure water and an aqueous solution of BAS or ovalbumin (1 g L^{-1}, pH = 7) were tested as feeds, respectively.

The water flux (J_w kg m^{-2} h) was calculated by the following equation:

$$J_w = \frac{M}{A \cdot \Delta t} \quad (2)$$

where M is the weight of permeated water, A the membrane area and Δt the permeation time.

Permeates were collected over a given period and weighed. The experiments were carried out at 25 °C. The BSA and ovalbumin rejection was determined using visible light-ultraviolet spectrophotometer (Spectrumlab 54, Lengguang Tech, China.). The rejection of protein (R, %) was obtained by:

$$R = \left(1 - \frac{C_p}{C_f}\right) \times 100 \quad (3)$$

where C_p and C_f are the ion concentrations in the permeate and feed, respectively.

Antifouling properties of prepared membrane

Protein solution (BSA, 200 mg L^{-1}, pH = 7) was used to test the antifouling properties of the prepared membrane. The flux of protein solution under 100 kPa was used to characterize the fouling level. The test process was carried out as follows: step 1, the pure water flux was measured and recorded 6 times for 2 h; step 2: the pure water was replaced by BSA solution and the flux for protein solution was also recorded 6 times for 2 h; step 3: step 2 was repeated; step 4: the measurement was completed with another pure water rinse. The flux recovery ratio (R_F, %) was calculated by:

$$R_{F_i} = \frac{F_i}{F_0} \times 100 \quad (4)$$

where F_0 and F_i are the fluxes of the original membrane and the BSA-fouling membrane, respectively; i is the circle of BSA-fouling.

Results and discussion

Dimethylacetamide was selected as one of the best solvents in the preparation of the iGO-doped PSF casting solution because of the good dispersion of iGO in this polar aprotic solvent, as reported by Stankovich.[19] The good dispersion of iGO in the membrane results in a good extended state for iGO, which is conducive to improving the mechanical properties of the membrane.

Characterization of GO and isocyanate-treated GO

Photographs of GO and iGO dispersed in water and DMAC (about 500 μg L^{-1}) are shown in Fig. 2a. The GO solutions appeared as an opaque brown color while the iGO solutions materialized a dark brown color. The different colors originated from the modification of the carboxyl and hydroxyl groups in GO *via* the formation of amides and carbamate esters, respectively. After sonication for 1 h, both GO and iGO had a good dispersion in DMAC. As in water, GO presented good dispersion but iGO still had very poor dispersion with visible particles suspended, and this is consistent with the prevenient report.[19] After being maintained stationary for 2 h, both the GO in DMAC and iGO in water precipitated by a significant portion, especially the later. Some small GO particles can be identified in the GO suspension, but no visible particles appeared in the iGO–DMAC suspension. Additionally, iGO suspension remained homogeneous for several weeks and then precipitation could be observed.[19] However, it seems that this phenomenon caused no negative effect on our experiment, because the iGO suspensions were used immediately after preparation. The SEM images of GO (Fig. 2b) and iGO (Fig. 2c) show a smooth surface

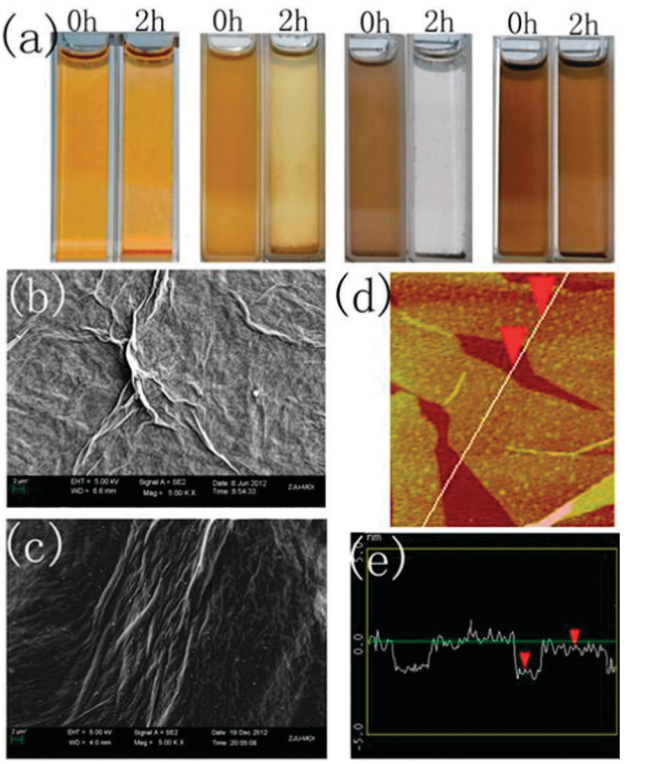

Fig. 2 (a) Photographs of GO and iGO dispersed in water or DMAC for 0 h or 2 h (from left to right: GO in water, GO in DMAC, iGO in water and iGO in DMAC). SEM images of GO (b) and iGO (c) nanosheets dried on a silicon wafer. AFM height image (d) of GO nanosheets dried on silicon wafer and the corresponding height profile (e) of the AFM image.

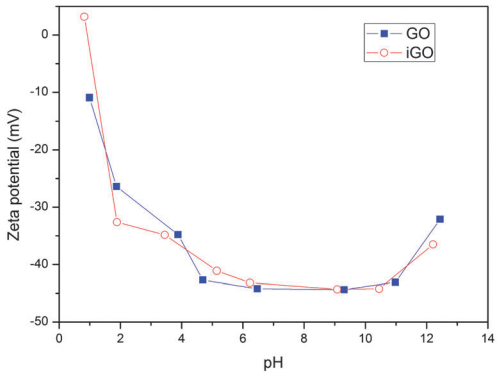

Fig. 3 Zeta potential of GO and iGO dispersed in water with different pH values.

with small wrinkles and no distinct changes in the morphology of the GO and iGO surfaces. An atomic force microscopy (AFM) image shows the profile of GO nanosheets dried on a silicon wafer. The thickness of GO is around 1 nm (Fig. 2c), indicating the existence of single-layer GO sheets.

The GO and iGO were dispersed in water (about 50 μg L^{-1}) to measure the zeta potential of hydrated particles after 1 h of ultrasonic treatment. GO and iGO were homogeneously suspended during the measurements, and the results are shown in Fig. 3. The value of the zeta potential is almost the same between GO and iGO, which is probably due to the fact that only a very small part of the carbonyl groups reacted with isocyanate, and the isocyanate mainly reacted with the hydroxyl groups in GO. This hypothesis will be confirmed by the XPS spectra analysis in the following text. The zeta potentials of GO and iGO decreased as the pH increased, which verifies the fact that the ionization of carboxylic groups is highly dependent on pH. When the pH was lower than 1, the zeta potential increased dramatically. The zeta potential is below −30 mV at a pH greater than 3 and lower than 11, and can reach −44.35 when the pH is 9.31, which is in good agreement with Li's report.[5]

In Stankovich's explanation,[19] the treatment of GO with organic isocyanate can lead to the derivatization of both edge carboxyl and surface hydroxyl functional groups *via* the formation of amides or carbamate esters, respectively. FTIR spectra in Fig. 4 verify the changes occurring in the GO treatment with 4-acetylphenyl isocyanate. The appearance of a strong absorption at 1704 cm^{-1}, corresponding to the C═O stretching vibration at 1733 cm^{-1} in GO, can be attributed to the carbonyl stretching vibration of carbamate esters of the surface hydroxyls in iGO.[19] Furthermore, the new absorption peak at 1664 cm^{-1} can originate from an amide carbonyl-stretching mode. The new stretch of 1522 cm^{-1} can probably be assigned to either amides or carbamate esters, and corresponds to the coupling of C–N stretching vibration with the CHN deformation vibration. Additionally, the FTIR spectrum of iGO shows no signal associated with the isocyanate group (2275–2263 cm^{-1}, as shown in the inset figure), indicating that the isocyanate treatment of GO leads to the chemical reactions and not the absorption or intercalation of organic isocyanate.

In order to investigate the effect of isocyanate treatment on the carbon structure of GO, Raman spectroscopy was employed,

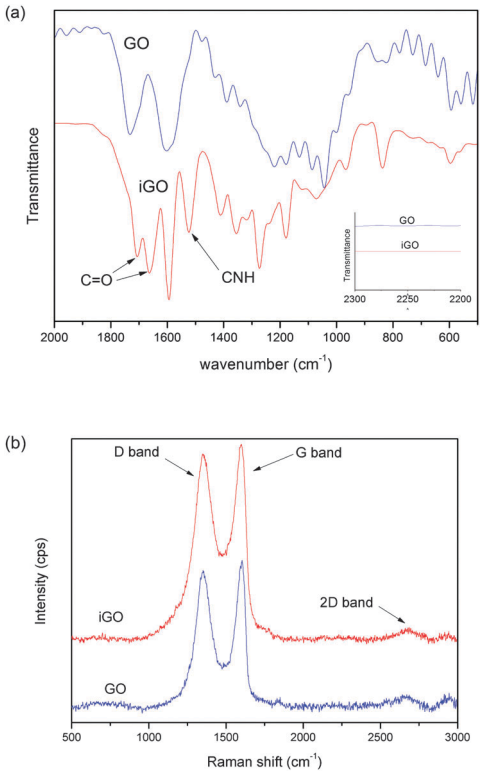

Fig. 4 FTIR spectra (a) and Raman spectra (b) of GO and iGO.

as shown in Fig. 4b. As is well-known, Raman spectroscopy is widely used as an efficient technique to detect the ordered–disordered crystal structures of GO.[43,44] The characteristics of Raman spectra of carbon-based materials are the D and G bands (~1350 and 1580 cm^{-1}), which originate from the local defects and the sp^2 graphitized segment in the structure, respectively.[43] Therefore, I_D/I_G peak intensity ratios are assigned to indicate the extent of disorder. The Raman spectrum shown in Fig. 4b displays the D and G peaks at about 1352 and 1595 cm^{-1}, respectively. Isocyanate treatment resulted in a small change in I_D/I_G ratio from 0.97 for GO to 0.94 for iGO, indicating a negligible decrease in the average size of the sp^2 domains, and also indicating that barely any new defect domains were created after isocyanate treatment. Additionally, according to the analysis of Raman spectra, it is also possible to speculate the single-, bi-, and multi-layer structures of graphene and GO, based on the shape and position of the 2D band.[45,46] In this work, the 2D bands of GO and iGO are centered at 2677 cm^{-1} with a very slight intensity but quite similar to the typical peak (2679 cm^{-1}), indicating that the existence of single layer structure does not obviously change compared to the pristine GO.

Fig. 5c gives the semiquantitative analysis of carbon (C), oxygen (O) and nitrogen (N) as calculated by area integral, listed in Table 1. Obviously, the element N has an enhanced amount increase, indicating the appearance of amide and carbamate ester. A small peak at ~175 eV in both the GO and iGO XPS spectra is a sign of the appearance of the element sulfur (S), which is probably introduced during the preparation and is not worth considering after isocyanate treatment.

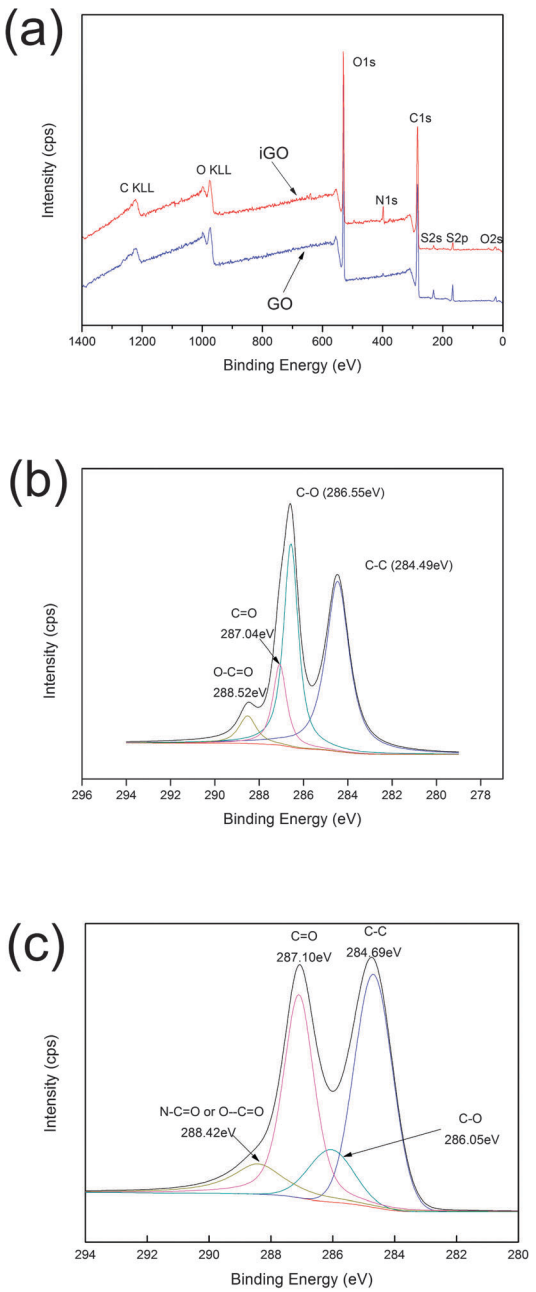

Fig. 5 XPS spectra for GO and iGO. Wide spectrum of GO and iGO (a), high-resolution C1s peaks of GO (b) and iGO (c).

Table 1 Semiquantitative analysis of elements in GO and iGO by XPS

	Atomic concentration (%)			Mass concentration (%)		
Elements	C	O	N	C	O	N
GO	63.34	35.66	1.00	56.55	42.41	1.04
iGO	66.15	29.92	3.94	59.82	36.06	4.15

For both GO and iGO, the high-resolution C1s XPS specta of GO and iGO sheets showed two distinct peaks (Fig. 5a and b, respectively): one peak at a lower binding energy, corresponding to the C–C and C–H bonding assigned at 284.5–285 eV, and the other quite prominent peak at higher binding energies, corresponding to large amounts of sp^3 carbon with C–O bonds (~286.5 eV), carbonyls (C═O, ~287.1 eV)), and carboxylates (O–C═O/N–C═O, ~289 eV), resulting from the appearance of heteroatoms and the destruction of the sp^2 atomic structure of graphene. However, the prominent peak at 286.55 eV in the C1s spectrum of GO (Fig. 5a) decreased dramatically after isocyanate treatment, while the peak at 287.1 eV increased inversely. This distinct change can be attributed to the replacement of hydroxyl by carbamate ester, which reduces the amount of hydroxyl and correspondingly augments the amount of carboxyl (reaction 2 in Fig. 1).

On the other hand, for the reaction between carboxyl and isocyanate, the amount of carbonyls remains constant, as shown in reaction 1 in Fig. 1. Additionally, the reactivity between hydroxyl and isocyanate is more significant compared to the reactivity between the carbonyls and isocyanate, in the sense that esterification reaction (between hydroxyl and isocyanate) is easier than anhydride synthesis between two acids (carboxyl and isocyanate, high temperature is usually needed) at room temperature.[46,47]

The characterization of iGO–PSF membranes

The hydrophilicity of the iGO–PSF membrane surfaces was characterized by the water contact angle and equilibrium water content. As can be seen in Fig. 6, for the blend membranes, the contact angle gradually decreased and equilibrium water content increased inversely when the amount of iGO was increased from 0.0% to 0.10% in the mixed membrane, indicating that the hydrophilicity of the blend membranes increases. This can be attributed to the fact that hydrophilic iGO migrates spontaneously to the membrane/water interface to reduce the interface energy during the phase inversion process.[30,48] This possible mechanism can also be verified by the different color between the top and bottom surfaces, which is originated from the top migration of iGO to the top-layer surface of the membrane, resulting in the top surface being black and the bottom surface being relatively lighter.[49]

However, when the amount of iGO in the blend membrane was increased to 0.15%, the water contact angle of the blend

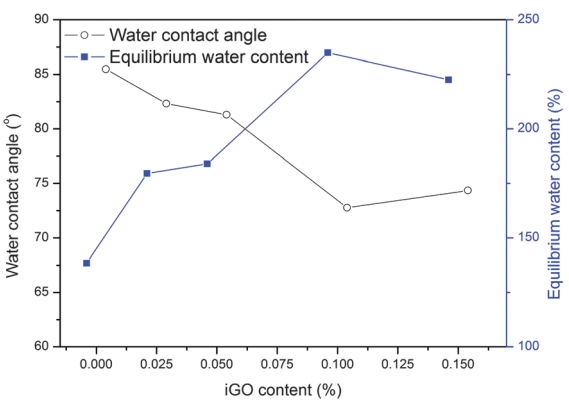

Fig. 6 Static water contact angle and equilibrium water content of the iGO–PSF mixed membranes.

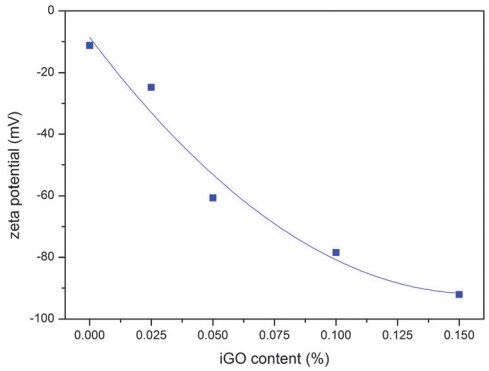

Fig. 7 Zeta potential of prepared membrane with different iGO contents.

membrane increased slightly and the equilibrium water content decreased, indicating that the hydrophilicity of the membrane decreased. This is probably due to the irregular position of iGO in the membrane structure at over 0.1% iGO content, as with the modified carbon nanotubes in our previous report in that a high content of carbon nanotubes leads to aggregation and reduces the effective surface of the nanotubes.[30]

The zeta potential of the prepared membrane was investigated to characterize the effect of doped iGO on the surface charge of the membrane, as shown in Fig. 7. The zeta potential decreased dramatically once iGO is added, and this is reasonably attributed to negatively charged iGO, as confirmed by the zeta potential of GO–iGO particles in Fig. 3. As the amount of iGO increased, massive iGO carrying abundant carboxyl groups appeared in the surface layer. After the prepared membranes were immersed in water, the carboxyl groups were hydrolyzed, resulting in the change of the zeta potential on the membrane's surface.

In order to investigate the effect of iGO on the blend membrane structure, the plane surface and cross-section of the prepared membranes were observed with scanning electron microscopy (SEM), as shown in Fig. 8. From Fig. 8a to e, the SEM images show that the sizes of the surface pores obviously diminished, and the surface became much smoother by addition of iGO species. Usually, the surface morphology is affected by the hydrophilicity of the additive (here iGO) and the viscosity of the casting solution,[50] and the effect of different nano-particles on the membrane surface is quite considerable. During the preparation of CNT-blended membranes,[30,49] a low CNT load increased the exchange between solvent and non-solvent, facilitating CNT collocation and thus roughened the surface, while a high CNT loading increased the viscosity and retarded the exchange of solvent and non-solvent, effectively smoothing the membrane surface and slowing down the precipitation of the membrane. However, in this experiment the viscosity of the casting solution seemed to dramatically increase once the iGO was added, and played a prominent role in deciding the morphology of the membrane, resulting in small surface pores and a smooth membrane surface. The conspicuous effect of iGO on the viscosity of the casting solution probably originated from the quite large specific surface of graphene compared to CNT. As the amount of iGO increased, some spots appeared in a deep color compared to the

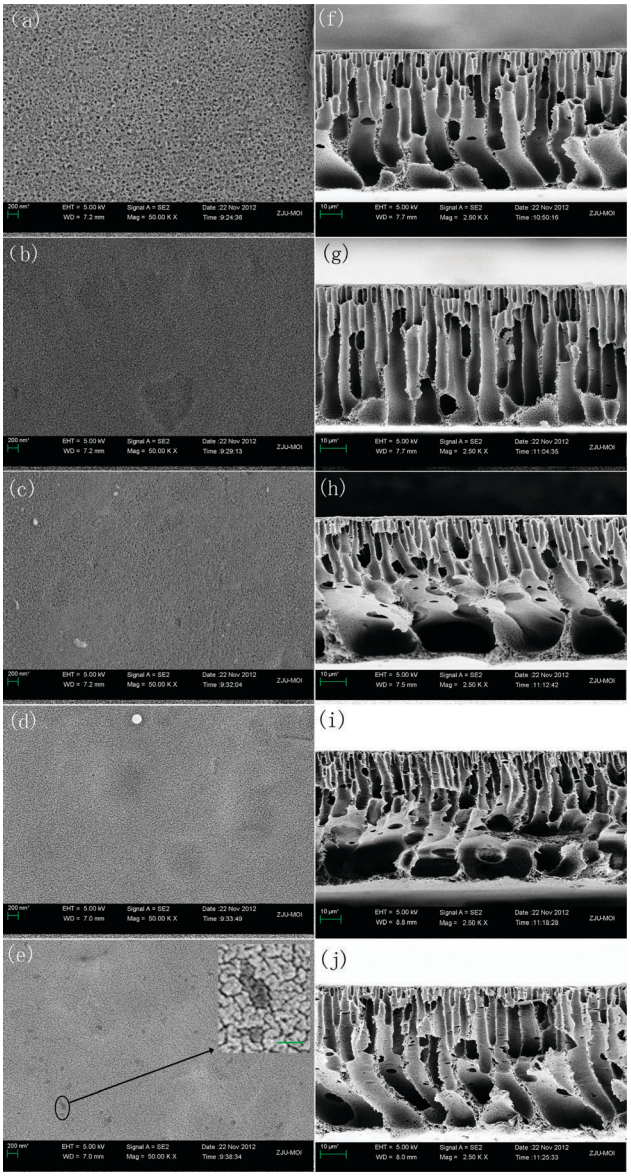

Fig. 8 SEM photographs of plane (a–e) and cross-sections (f–j) of membranes with different iGO contents of 0.0, 0.025, 0.05, 0.10, and 0.15%.

bulk surface of the membrane, especially the membrane with 0.15% iGO content. The sporadic spots were believed to be the shadows of graphene clusters. However, the uniform distribution of the spots also indicated a good dispersion of iGO in the casting solution.

Fig. 8f–j show cross-sections of membranes prepared from 0, 0.025, 0.05, 0.10, and 0.15%. The structure of the membrane with no iGO blended is generally asymmetric with numerous macro-voids (sub layer) and a dense thick top layer. There is an obvious change in the sub layer of the membranes after the addition of iGO. The membrane prepared by 0.025% iGO–PSF has straight and slightly more finger-like micro-voids, which may benefit from the enhanced exchange of solvent and non-solvent during the phase inversion. It seems paradoxical compared with the appearance of the smooth surface, which resulted from the retarded exchange between solvent and non-solvent due to

increased viscosity. We proposed a mechanism to explain this phenomenon: the exchange between the solvent and non-solvent during phase inversion does improve, however slightly, in that it has a positive effect on the cross-section structure (producing straighter and more finger-like micro-voids), although a different effect on the surface (producing small pores but a smooth surface). With the iGO content increasing, huge voids and pore wall with cracks appear in the sub layer, similar to the fabrication of the CNT–PSF membrane as reported by Vatanpour.[49]

AFM was used for morphological characterization of the membrane surface for complementary information, as shown in Fig. 9, including both plane and three-dimensional AFM images.

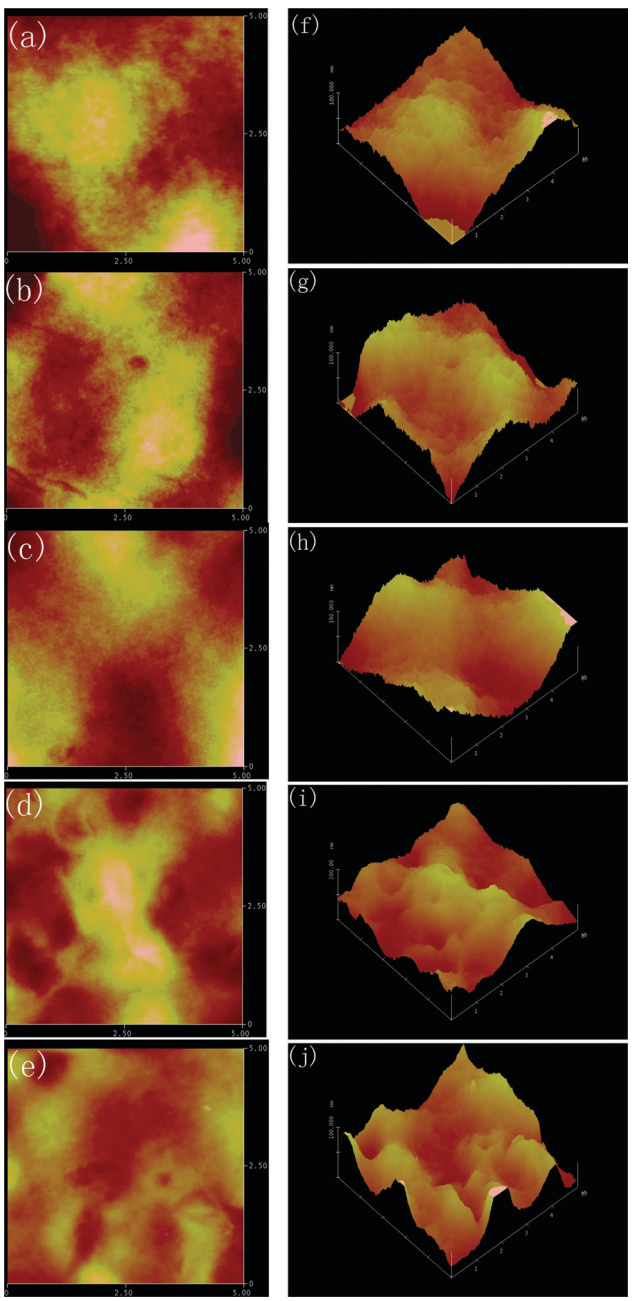

Fig. 9 The plane (a–e) and three-dimensional (f–j) images of AFM of prepared membranes with iGO contents of 0.0, 0.025, 0.05, 0.10, and 0.15%.

According to the AFM images, the pristine PSF membrane surface is quite rough and the iGO blend membrane with a content of 0.05% is overtly smoother, as in our previous MWNTs–PSF membrane.[30] However, after the content of iGO was increased to 0.15%, evident valleys appeared although the smoothness of the local surface area barely changed.

Separation performance of prepared membrane

The pure water flux and the separation performance of prepared membranes are plotted in Fig. 10. By blending a slight content of iGO in the casting solution (0.025%), the pure water flux of the PSF membrane was improved. When the iGO content increased, the flux gradually decreased. This trend is also quite similar to our previous report on the performance of CNT–PSF membranes.[30] For the enhancement of flux with a small iGO content, this can be explained as the result of an improvement in the hydrophilicity of the membrane and the formation of straight and a slightly more finger-like micro-voids. As the iGO content exceeds 0.05%, the aggregation of iGO during the phase inversion process increased the viscosity of the casting solution and greatly reduced the porosity of the membrane, as shown in Fig. 8a–e. Furthermore, the shades appearing in Fig. 8e indicate that the effective area of the membrane decreased, because the graphene sheets are waterproof. Even though the gap between the graphene sheets has an incomparable selectivity for water, the permeability is significantly small.[28]

Protein retention measurements with BSA and ovalbumin at a pressure difference of 100 kPa were carried out with cross-flow cell modules at pH 7. The rejections of the prepared membrane were about 95% for BSA and about 6% for ovalbumin, with no distinct relationship with increasing iGO content (Fig. 10). However, this does not mean that the addition of iGO has no effect on the prepared membrane pores. In our previous experiment,[30] the surface mean pore size became larger with increasing MWNT content, resulting in a decrease in the rejection of PEG-20 000. In this experiment, the surface mean pore size became smaller with increasing iGO content, which is probably due to the different structure and effect between MWNT and iGO as explained above. But the change in pore size caused by the addition of iGO is not big enough to affect protein rejection, leading to an inconspicuous

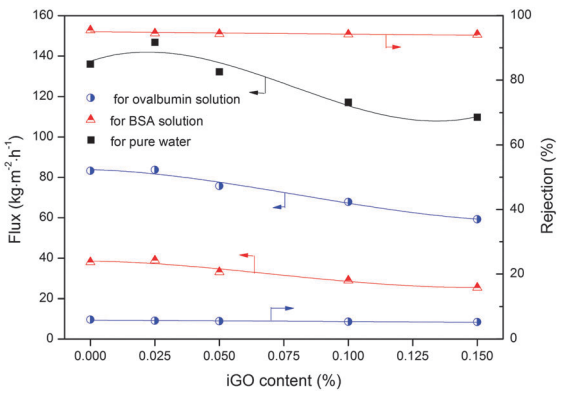

Fig. 10 Separation performance of prepared membrane.

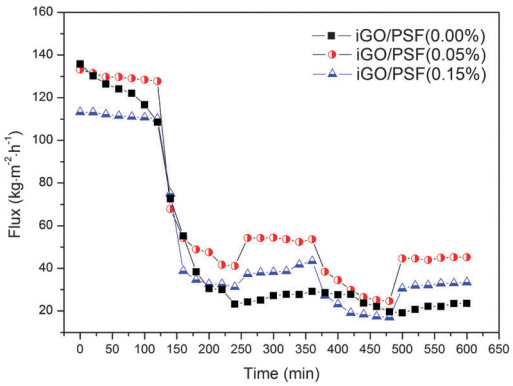

Fig. 11 Flux *versus* time for iGO blended PSF membranes at 100 kPa.

relationship with increasing iGO content. The prepared membrane rejections were about 95% for BSA and about 6% for ovalbumin, indicating the molecular weight cut-off (MWCO) of the prepared membranes was between 4500 and 6700.

Antifouling property of prepared of membrane

Generally, the flux decrease indicates that the fouling process occurred on the membrane,[51] during which the electrostatic force, hydrogen bonding and hydrophobic force and Van der Waals forces are responsible for the fouling of the membrane surface.[52] We recorded the flux changes for 10 h in pure water or alternating BSA solution every 2 h, as shown in Fig. 11. The flux recovery ratio of the prepared membranes after BSA fouling was calculated and is listed in Table 2.

The flux recovery ratio of the iGO blend membranes is obviously higher than that of the pristine membrane. The pristine PSF membrane flux recovery ratios were only 21.51% and 17.32% in the first and second cycles, respectively. The low recovery ratio indicated the poor antifouling property of the pristine membrane. On the other hand, the flux recovery ratios of the iGO blend (0.05%) membranes were 40.27% cycles, respectively. And the flux recovery ratio of the iGO blend (0.15%) membrane decreased slightly compared with the former.

The improved antifouling property of the prepared membranes can be attributed to increasing hydrophilicity, a more negative zeta potential and an improved smoothness of the membrane surface as shown in Fig. 6, 7 and 9.

The increasing of hydrophilicity of the membranes prepared with iGO (Fig. 6) originated from bonding ionized carboxylic groups in the iGO surface with a water layer in the aqueous solution is one reason for preventing protein adsorption on the surfaces of the prepared membranes.[49]

Table 2 Flux recovery ratio of prepared membranes

iGO content (%)	R_{F1}[a] (%)	R_{F2}[a] (%)
0.00	21.51	17.32
0.05	40.27	33.96
0.15	38.33	29.51

[a] R_{F1} and R_{F2} denote the flux recovery ratio in first and second cycles.

The effect of membrane surface charge on the fouling process seems well-established, and the repulsive forces existing between the charged surface and co-ions in the feed solution prevent solute deposition on the membrane surface, thus reducing fouling.[53] The charge on the membrane surface can be characterized by the zeta potential, which mainly depends on the nature of the ions present in the solution and the properties of the solid surface itself.[38] The zeta potential of the prepared membrane decreased dramatically as the iGO content increased, as shown in Fig. 7. In our experiments, the pH value of the BSA solution was 7 and the BSA molecules were negatively charged because the isoelectric point of BSA is about 4.9. The surface of the membrane contains abundant iGO, in that hydrophilic iGO migrates to the membrane/water interface during the phase inversion process as described above.

It is generally deemed that the AFM analysis can provide an established correlation between surface roughness and fouling, which means fouling increases with an increase in surface roughness.[53] Foulants are likely to be absorbed in the valleys of the membrane,[54] thus antifouling can be enhanced by an increase in the surface smoothness. Unfortunately, the established correlation is only suitable for a limited range of RO and NF membranes and it is not certain whether the correlation can be extrapolated to a wider range of membrane roughness. In our experiments, the smoothness of the membrane, which is best improved after the addition of iGO (0.05%, as shown in Fig. 9c), corresponds to an improved antifouling property. Once the content of iGO was increased to 0.15% (Fig. 9j) evident valleys appeared, although the smoothness of the local surface area barely changed, resulting in a slightly minimized flux recovery ratio.

Conclusion

Graphene oxide (GO) was modified by isocyanate, and the resultant isocyanate-treated GO (iGO) was well-dispersed in organic solvent. FITR spectrum and XPS analyses confirmed the existence of isocyanate groups in the GO, and Raman spectrum showed no relevant change occurred in the GO structure after the treatment. After the addition of iGO to the PSF membrane, the hydrophilicity of the prepared membranes increased and the zeta potential of the prepared membranes became more negative with an increasing iGO content. SEM and AFM analyses showed that the surface pores of the prepared membrane were minimized, but the pore structure and the surface smoothness was improved with proper iGO content. Compared to the bare PSF membrane, the flux of the iGO–PSF membrane increased with a small content of iGO and then decreased with massive iGO content. The rejections of the prepared membrane were about 95% for BSA and about 6% for ovalbumin and this indicates the molecular weight cut-off of the prepared membranes is between 4500 and 6700. The antifouling property of the iGO–PSF membranes were greatly improved by the addition of iGO, and this can be attributed to enhanced hydrophilicity, improved surface smoothness and the more negative zeta potential of the prepared membrane.

Acknowledgements

This work was supported by the National Natural Science Foundation of China (21076176, 21076190); the National Basic Research Program of China (2009CB623402); and the Scientific & Technological Innovation Team of Zhejiang Province (2009R50045).

Notes and references

1 K. S. Novoselov, A. K. Geim, S. V. Morozov, D. Jiang, Y. Zhang, S. V. Dubonos, I. V. Grigorieva and A. A. Firsov, *Science*, 2004, **306**, 666.
2 A. K. Geim and K. S. Novoselov, *Nat. Mater.*, 2007, **6**, 183.
3 J. C. Meyer, A. K. Geim, M. I. Katsnelson, K. S. Novoselov, T. J. Booth and S. Roth, *Nature*, 2007, **446**, 60.
4 S. Stankovich, D. A. Dikin, G. H. B. Dommett, K. M. Kohlhaas, E. J. Zimney, E. A. Stach, R. D. Piner, S. T. Nguyen and R. S. Ruoff, *Nature*, 2006, **442**, 282.
5 D. Li, M. B. Muller, S. Gilje, R. B. Kaner and G. G. Wallace, *Nat. Nanotechnol.*, 2008, **3**, 101.
6 R. Ruoff, *Nat. Nanotechnol.*, 2008, **3**, 10.
7 D. R. Dreyer, S. Park, C. W. Bielawski and R. S. Ruoff, *Chem. Soc. Rev.*, 2010, **39**, 228.
8 Y. Zhang, Y. W. Tan, H. L. Stormer and P. Kim, *Nature*, 2005, **438**, 201.
9 S. Garaj, W. Hubbard, A. Reina, J. Kong, D. Branton and J. A. Golovchenko, *Nature*, 2010, **467**, 190.
10 A. A. Balandin, S. Ghosh, W. Bao, I. Calizo, D. Teweldebrhan, F. Miao and C. N. Lau, *Nano Lett.*, 2008, **8**, 902.
11 C. Lee, X. Wei, J. W. Kysar and J. Hone, *Science*, 2008, **321**, 385.
12 S. Stankovich, D. A. Dikin, R. D. Piner, K. A. Kohlhaas, A. Kleinhammes, Y. Jia, Y. Wu, S. T. Nguyen and R. S. Ruoff, *Carbon*, 2007, **45**, 1558.
13 Z. Sun, D. K. James and J. M. Tour, *J. Phys. Chem. Lett.*, 2011, **2**, 2425.
14 W. S. Hummers and R. E. Offeman, *J. Am. Chem. Soc.*, 1958, **80**, 1339.
15 D. C. Marcano, D. V. Kosynkin, J. M. Berlin, A. Sinitskii, Z. Sun, A. Slesarev, L. B. Alemany, W. Lu and J. M. Tour, *ACS Nano*, 2010, **4**, 4806.
16 S. Niyogi, E. Bekyarova, M. E. Itkis, J. L. McWilliams, M. A. Hamon and R. C. Haddon, *J. Am. Chem. Soc.*, 2006, **128**, 7720.
17 A. B. Bourlinos, D. Gournis, D. Petridis, T. Szabó, A. Szeri and I. Dékány, *Langmuir*, 2003, **19**, 6050.
18 H. Bai, Y. Xu, L. Zhao, C. Li and G. Shi, *Chem. Commun.*, 2009, 1667.
19 S. Stankovich, R. D. Piner, S. T. Nguyen and R. S. Ruoff, *Carbon*, 2006, **44**, 3342.
20 D. A. Dikin, S. Stankovich, E. J. Zimney, R. D. Piner, G. H. B. Dommett, G. Evmenenko, S. T. Nguyen and R. S. Ruoff, *Nature*, 2007, **448**, 457.
21 W. Lv, C. H. You, S. Wu, B. Li, Z. P. Zhu, M. Wang, Q. H. Yang and F. Kang, *Carbon*, 2012, **50**, 3233.
22 H. Chen, M. B. Müller, K. J. Gilmore, G. G. Wallace and D. Li, *Adv. Mater.*, 2008, **20**, 3557.
23 O. Akhavan and E. Ghaderi, *ACS Nano*, 2010, **4**, 5731.
24 W. Hu, C. Peng, W. Luo, M. Lv, X. Li, D. Li, Q. Huang and C. Fan, *ACS Nano*, 2010, **4**, 4317.
25 X. Cai, S. Tan, M. Lin, A. Xie, W. Mai, X. Zhang, Z. Lin, T. Wu and Y. Liu, *Langmuir*, 2011, **27**, 7828.
26 S. Liu, T. H. Zeng, M. Hofmann, E. Burcombe, J. Wei, R. Jiang, J. Kong and Y. Chen, *ACS Nano*, 2011, **5**, 6971.
27 W. P. Xu, L. C. Zhang, J. P. Li, Y. Lu, H. H. Li, Y. N. Ma, W. D. Wang and S. H. Yu, *J. Mater. Chem.*, 2011, **21**, 4593.
28 R. R. Nair, H. A. Wu, P. N. Jayaram, I. V. Grigorieva and A. K. Geim, *Science*, 2012, **335**, 442.
29 E. N. Wang and R. Karnik, *Nat. Nanotechnol.*, 2012, **7**, 552.
30 S. Qiu, L. Wu, X. Pan, L. Zhang, H. Chen and C. Gao, *J. Membr. Sci.*, 2009, **342**, 165.
31 S. Qiu, L. Wu, G. Shi, L. Zhang, H. Chen and C. Gao, *Ind. Eng. Chem. Res.*, 2010, **49**, 11667.
32 A. Al-Amoudi, P. Williams, S. Mandale and R. W. Lovitt, *Sep. Purif. Technol.*, 2007, **54**, 234.
33 T. Xu, R. Fu and L. Yan, *J. Colloid Interface Sci.*, 2003, **262**, 342.
34 M. Mullet, P. Fievet, J. C. Reggiani and J. Pagetti, *J. Membr. Sci.*, 1997, **123**, 255.
35 A. Martín, F. Martínez, J. Malfeito, L. Palacio, P. Prádanos and A. Hernández, *J. Membr. Sci.*, 2003, **213**, 225.
36 M. S. Chun, H. I. Cho and I. K. Song, *Desalination*, 2002, **148**, 363.
37 M. Ernst, A. Bismarck, J. Springer and M. Jekel, *J. Membr. Sci.*, 2000, **165**, 251.
38 D. B. Burns and A. L. Zydney, *J. Membr. Sci.*, 2000, **172**, 39.
39 I. H. Huisman, E. Vellenga, G. Trägårdh and C. Trägårdh, *J. Membr. Sci.*, 1999, **156**, 153.
40 G. Hagmeyer and R. Gimbel, *Sep. Purif. Technol.*, 1999, **15**, 19.
41 D. Möckel, E. Staude, M. Dal-Cin, K. Darcovich and M. Guiver, *J. Membr. Sci.*, 1998, **145**, 211.
42 W. R. Bowen and X. Cao, *J. Membr. Sci.*, 1998, **140**, 267.
43 A. C. Ferrari and J. Robertson, *Phys. Rev. B: Condens. Matter*, 2000, **61**, 14095.
44 A. C. Ferrari, J. C. Meyer, V. Scardaci, C. Casiraghi, M. Lazzeri, F. Mauri, S. Piscanec, D. Jiang, K. S. Novoselov, S. Roth and A. K. Geim, *Phys. Rev. Lett.*, 2006, **97**, 187401.
45 Z. H. Gao, J. Y. Gu, X. M. Wang, Z. G. Li and X. D. Bai, *Pigm. Resin Technol.*, 2005, **34**, 282.
46 C. Zhao, L. Ji, H. Liu, G. Hu, S. Zhang, M. Yang and Z. Yang, *J. Solid State Chem.*, 2004, **177**, 4394.
47 I. S. Blagbrough, N. E. Mackenzie, C. Ortiz and A. I. Scott, *Tetrahedron Lett.*, 1986, **27**, 1251.
48 E. Celik, H. Park, H. Choi and H. Choi, *Water Res.*, 2011, **45**, 274.
49 V. Vatanpour, S. S. Madaeni, R. Moradian, S. Zinadini and B. Astinchap, *J. Membr. Sci.*, 2011, **375**, 284.
50 J. H. Choi, J. Jegal and W. N. Kim, *J. Membr. Sci.*, 2006, **284**, 406.
51 L. Song, *J. Membr. Sci.*, 1998, **139**, 183.
52 S. Boributh, A. Chanachai and R. Jiraratananon, *J. Membr. Sci.*, 2009, **342**, 97.
53 D. Rana and T. Matsuura, *Chem. Rev.*, 2010, **110**, 2448.
54 A. Razmjou, J. Mansouri and V. Chen, *J. Membr. Sci.*, 2011, **378**, 73.

